ACS NANO

www.acsnano.org

ARTICLE

Near-Field Thermal Radiation as a Probe of Nanoscale Hot Electron and Phonon Transport

Mohammad Habibi, Albert Beardo, and Longji Cui*

Cite This: *ACS Nano* 2025, 19, 6033–6043

Read Online

ACCESS | Metrics & More | Article Recommendations | Supporting Information

ABSTRACT: **Understanding the energy transport properties of hot energy carriers is of great importance for a diverse range of topics from nanoelectronics and photochemistry to the discovery of quantum materials. While much progress has been made in the study of hot carrier dynamics using ultrafast far-field time-resolved spectroscopies, it remains a great challenge to understand hot carrier transport and interaction dynamics at the nanoscale. Existing theoretical models yield only qualitative predictions that are difficult to validate against experiments. Here we present a theoretical framework that extends the study of near-field thermal radiation into the ultrafast time domain, enabling sensitive local probing and quantitative study of nanoscale hot electron and phonon transport effects that have been challenging to quantify. The proposed technique of near-field hot carrier nanoscopy directly links the features of different nonequilibrium effects to near-field thermal absorption and scattering by a scanning nanotip. Our model predicts ultrafast thermal radiation in response to photoexcitation, as well as elucidates the nanoscopic radiation properties of a number of hot carrier dissipation pathways, including nonlinear electron supercollision, second sound, and nonlocal phonon transport. This work is expected to guide experiments to identify the fundamental constraints unlocking thermal wave (second sound) propagation and address the roles of competing hydrodynamic and ballistic phonon effects at the nanoscale.**

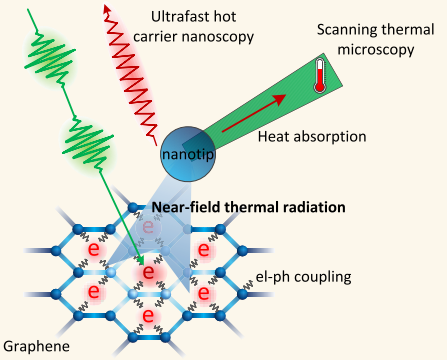

KEYWORDS: *hot carriers, near-field thermal radiation, phonon hydrodynamics, electron−phonon coupling, second sound*

INTRODUCTION

Hot electron and phonon phenomena are prevalent in the study of materials physics and device applications. Under intense optical and electrical excitations, electronic and vibrational subsystems can be driven separately into highly nonequilibrium states and then undergo rapid relaxations via coherent and incoherent interactions within and among different carriers. Understanding these phenomena has played a vital role in the development of modern semiconductor devices[1] and holds great interest for enhancing photovoltaics,[2] light emission,[3] photosensing,[4] thermoelectrics,[5] and chemical reactions.[6] Recent advances have extended beyond classical materials, revealing the role of hot carriers in the formation of distinct phases in quantum materials.[7−9] While carrier dynamics has been extensively investigated via time-resolved pump−probe spectroscopies with ultrahigh temporal resolution,[10−13] the diffraction-limited spatial resolution of far-field characterization hinders studies at the nanoscale—the intrinsic length scale where hot carrier processes occur. Nanoscopic imaging of energy transport and interactions could help discern the role of hot electrons in mediating plasmon photochemistry,[6] and clarifying the interplay of heat inertia and ballistic or viscous non-Fourier phonon transport.[14−17]

Near-field optical[18−20] and thermal microscopies[21−24] can overcome the limitations in nanoscale hot carrier imaging. In principle, by positioning a nanotip in close proximity to the carriers, highly localized transport properties can be mapped by detecting either scattered or absorbed near-field thermal and optical energy. As a result, hot electrons and phonons can be monitored passively with minimal perturbation, which has been a difficult task using ultrafast laser techniques, as the probing light disturbs the hot electrons due to their minute heat capacity. Despite fundamental interests, a rigorous theory to understand the interactions between near-field photonic modes and hot carriers has not yet been established. The study of near-field radiative heat transfer has been mainly centered on equilibrium systems.[25−33] Previous attempts have made assumptions to approximate near-field energy exchange and hot carrier processes separately,[34,35] resulting in predictions that are not directly comparable with experiments, or they have

Received: August 27, 2024
Revised: January 29, 2025
Accepted: January 31, 2025
Published: February 10, 2025

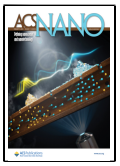

Downloaded via UNIV OF COLORADO BOULDER on February 19, 2025 at 23:01:47 (UTC).
See https://pubs.acs.org/sharingguidelines for options on how to legitimately share published articles.

ACS Publications

© 2025 American Chemical Society

https://doi.org/10.1021/acsnano.4c11893
ACS Nano 2025, 19, 6033−6043

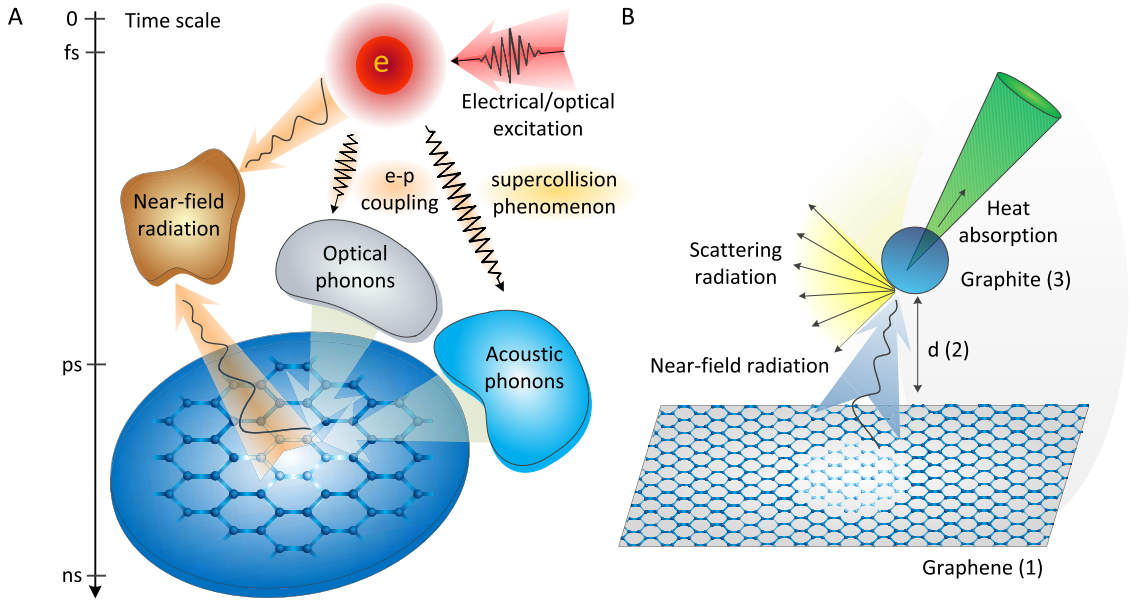

Figure 1. (A) Various hot electron and phonon processes studied in this work and the relevant time scales. (B) Schematics for near-field thermal energy transfer (absorption and scattering) between hot carriers in monolayer graphene and a spherical nanotip.

focused on steady-state situations,[18−20] preventing the observation of the transient mechanisms that govern carrier evolution far from equilibrium. Recent theoretical work has studied the interplay between near-field thermal radiation and heat conduction in the extreme near field either within the framework of steady-state phonon conduction or slower dipole dynamics,[36−38] but not in the context of ultrafast hot carrier transport and hydrodynamics. In this article, we propose the concept of near-field hot carrier nanoscopy to study both hot electron and phonon transport behavior at the nanoscale and in the ultrafast time domain. A nonequilibrium near-field thermal energy transfer theory is presented to directly link local hot carrier transport within a material and the near-field thermal absorption and scattering by a nanotip close to the hot carriers. The model is illustrated by considering ultrafast laser excitation in monolayer graphene (the model material system studied in this work) and serves as the theoretical foundation for leveraging near-field radiative thermal effects as nanoscale probes to quantitatively elucidate hot carrier dynamics, cooling pathways, and related phenomena, such as electron supercollision[39,40] and phonon hydrodynamics.[41−43]

RESULTS AND DISCUSSION

Theoretical Model. The hot carrier and near-field thermal radiation processes are depicted in Figure 1A. Carriers can be excited either transiently by an ultrafast laser pulse or pumped to a nonequilibrium steady state by continuous optical or electrical excitation. Thermal equilibration after excitation results from transport and scattering mechanisms involving excited hot electrons and phonons. This nonequilibrium evolution can be monitored spatially and temporally using a nanotip by measuring absorbed or scattered near-field radiation. We consider a spherical nanotip placed in the thermal near-field of hot carriers hosted within a monolayer graphene (Figure 1B). To relate hot carrier physics to the near-field thermal radiation, we use a generalized multitemperature model that distinguishes the temperature of hot electrons and different phonon branches[44,45] and accounts for the influence of phonon hydrodynamics[14] and electron supercollision[39]

$$C_e\frac{\partial T_e}{\partial t} = -\nabla\cdot\vec{q}_e - Q_e^{th}(T_e, T_t) - Q_e^{S} + Q_e^{l} - \sum_i G_{ep_i}^{n}(T_e - T_{p_i}) - \sum_i G_{ep_i}^{SC}(T_e^{\delta} - T_{p_i}^{\delta}) \quad (1)$$

$$C_{p_i}\frac{\partial T_{p_i}}{\partial t} = -\nabla\cdot\vec{q}_{p_i} - \phi_{p_i}Q_p^{th}(T_{lat}, T_t) - Q_{p_i}^{S} + Q_{p_i}^{l} + G_{ep_i}^{n}(T_e - T_{p_i}) + G_{ep_i}^{SC}(T_e^{\delta} - T_{p_i}^{\delta}) + G_{pp_i}(T_{lat} - T_{p_i}) \quad (2)$$

where T_e and T_{p_i} are the temperatures of electrons and i-th (i = 1−6) phonon branches, C_e, and C_{p_i} denote the specific heat capacities, and Q_e^l and $Q_{p_i}^l$ are the power densities injected by an ultrafast laser pulse into the electronic and phononic subsystems. Based on the intrinsic particle-hole symmetry of graphene, we model a single temperature T_e for both excited electrons and holes. We consider room-temperature initial conditions and a Gaussian-shape laser excitation with a pulse duration of 200 fs. Specifically, the laser power density absorption by the graphene layer follows a Gaussian distribution, $Q^l(r) = \frac{2.3\times10^{-11}}{2\pi t_{gr}L^2}e^{-1/2(r/L)^2}$, where t_{gr} = 0.335 nm is the thickness of the monolayer,[46] L is the focused spot size, and r is the radial distance from the center of the laser spot.[47] As shown later, choosing a small spot size L of a few hundred of nanometers, which requires the use of short wavelength light due to the diffraction limit, is critical for uncovering nondiffusive phonon transport effects in graphene at room temperature. As a reference, based on the dielectric functions of electrons and the different phonon branches and the resulting photoabsorption at the range of temperatures under study, and considering laser photon energies at around 3 eV, the absorbed power is ∼2% of the total laser power.[48,49] While electrons and optical phonons absorb 90 and 10% of Q^l, respectively, acoustic phonons are not directly excited. Moreover, the local absorption and scattered near-field energy

https://doi.org/10.1021/acsnano.4c11893
ACS Nano 2025, 19, 6033−6043

Table 1. Thermal Properties and Coupling Factors of Hot Electrons and Different Phonon Branches

properties	electron	LA	TA	ZA	LO	TO	ZO
κ ($W{\cdot}m^{-1}{\cdot}K^{-1}$)	50	863.0	237.9	2780.0	10.0	10.0	20.9
C ($MJ{\cdot}m^{-3}{\cdot}K^{-1}$)	0.00036	0.19	0.32	0.61	0.03	0.02	0.16
G_{ep}^{n} ($TW{\cdot}m^{-3}{\cdot}K^{-1}$)		100	1	0	600	2700	0
G_{ep}^{SC} ($MW{\cdot}m^{-3}{\cdot}K^{-1}$)		93.9	413.6	0	0	0	0
G_{pp} ($TW{\cdot}m^{-3}{\cdot}K^{-1}$)		2700	13000	1900	2700	1400	400
τ (ps)		70.8	24.7	317	10	12	388
l (μm)		1.42	0.494	6.34	0.2	0.24	7.76

by the tip at temperature T_t are denoted by $Q_{e/p}^{th}$ and $Q_{e/p}^{S}$, respectively, and ϕ_{p_i} represents the contribution of each phonon branch to near-field thermal radiation (see Supporting Information). Energy transfer between the electronic and phononic subsystems occurs via normal and supercollision electron−phonon scattering, and is proportional to the coupling factors $G_{ep_i}^{n}$ and $G_{ep_i}^{SC}$. In monolayer graphene, the supercollision effect indicates a nonlinear coupling between hot electrons and acoustic phonons. This effect is characterized by an exponent δ, which takes the value 1, 3, and 5 for $k_B T_e \ll \mu$, $k_B T_e < \mu$, and $k_B T_e > \mu$, respectively, where μ is the chemical potential and k_B is the Boltzmann constant.[39] For phonons, the coupling between different branches is described by the coupling factors $G_{pp_i} = \frac{C_{p_i}}{\tau_{p_i}}$, where τ_{p_i} is the average scattering time of the modes in the i-th branch. Finally, the conservation of energy, $\sum_i G_{pp_i}(T_{lat} - T_{p_i}) = 0$, is used to determine the global lattice temperature $T_{lat} = \frac{\sum G_{pp_i} \cdot T_{p_i}}{\sum G_{pp_i}}$.[45]

We note that (1) and (2) assume that the excited electron density remains constant during the experiment and neglect the energy transferred from electrons and holes to optical phonons due to nonradiative electron−hole recombination, which can take place at the ps scale in graphene.[50] First, in the present experiments the carrier concentration is not expected to be extremely high, thus limiting the frequency of recombination events. Second, not all of the energy lost during electron−hole recombination is transferred to the lattice. A significant fraction remains in the electronic subsystem via Auger processes or impact excitations, which can also operate at ps time scale in graphene.[51] Therefore, for simplicity, we neither consider an energy sink (source) term for electrons (phonons) that depends on the phonon-assisted electron−hole recombination rate, nor modifications of T_e due to a time-dependent electron density,[51] which would require explicitly modeling the carrier concentration via the diffusion-recombination equation.[52]

The constitutive heat transport equations, which relate the conductive heat fluxes ($\vec{q}_e$ and $\vec{q}_{p_i}$) and the temperatures of the corresponding hot carriers, depend on the time scale of interest. For electrons, we assume diffusive transport as described by Fourier's law

$$\vec{q}_e = -\kappa_e \nabla T_e \tag{3}$$

where κ_e is the electronic thermal conductivity. This is motivated by the significant reduction in the electron mean free path (MFP) due to defects and impurity scattering in realistic graphene samples.[53] However, longer MFPs have been reported for ultraclean samples,[54] which could lead to nondiffusive electron transport signatures.[55,56] In addition, we assume a constant and uniform chemical potential and electron diffusivity, which neglect many-body effects that can emerge under high carrier concentrations,[57] exciton diffusion,[58] and band gap shifts due to lattice temperature gradients.[59] While these effects are not expected to be dominant in the present experiments at room temperature with moderate laser fluences, they might be detectable using the proposed near-field hot carrier nanoscopy by adequately refining eq 3. For phonons, it is well established that a significant fraction of the phonon MFP spectrum is comparable to or larger than the laser spot sizes of hundreds of nanometers considered here, thus revealing ballistic or collective transport effects. The resulting nondiffusive mechanisms are accounted for by using a hydrodynamic-like transport equation[60,61]

$$\tau_{p_i}\frac{\partial \vec{q}_{p_i}}{\partial t} + \vec{q}_{p_i} = -\kappa_{p_i}\nabla T_{p_i} + l_{p_i}^2(\nabla^2 \vec{q}_{p_i} + \alpha \nabla(\nabla \cdot \vec{q}_{p_i})) \tag{4}$$

where α is a volume viscosity coefficient, κ_{p_i} is the lattice thermal conductivity, and l_{p_i} is the nonlocal length, estimated here for each branch as the average MFP. In contrast to the diffusive heat transport model used in refs 45,52, the non-Fourier effects in eq 4 allow the study of a number of unique phonon transport phenomena including phonon memory, viscosity, and vorticity.[14,41−43,62,63] As shown later, these hydrodynamic effects combined with linear and nonlinear electron−phonon coupling physics can be detected by the proposed near-field hot carrier nanoscopy with high spatiotemporal resolution.[42,43,63]

We numerically solve (1−4) using finite element methods implemented in COMSOL Multiphysics.[64] The thermal properties and coupling factors of hot electrons and the six different phonon branches are obtained from ref 45and listed in Table 1. We note that the present model could be refined by considering temperature-dependent material properties, particularly for the electron system that reaches high temperatures, but such nonlinearities are not expected to modify the phenomenology described below. Moreover, for all phonon branches, we assume a volume viscosity coefficient $\alpha = 2$ in eq 4, as obtained in the original derivation by Guyer and Krumhansl.[61] However, we note that using smaller values of α, as predicted by modern derivations,[15] would lead to a slight attenuation of the viscous nonlocal effects.

Near-field radiative heat exchange between the nanotip and the substrate is modeled using fluctuational electrodynamics.[25] Specifically, the radiative heat flux emitted from the substrate is obtained from the statistical averaging of the Poynting vector, $\langle \vec{S}(r, \omega)\rangle = 2\,\mathrm{Re}\langle \vec{E}(r, \omega) \times \vec{H}^*(r, \omega)\rangle$, at position r and frequency ω. The electric ($\vec{E}$) and magnetic ($\vec{H}$) fields originate from the local fluctuating currents ($j(r)$) associated with hot electrons and phonons. The fluctuation−dissipation

https://doi.org/10.1021/acsnano.4c11893
ACS Nano 2025, 19, 6033−6043

theorem (FDT) can then be applied to relate the correlated fluctuating currents to the optical properties of the materials[65]

$$\begin{aligned}\langle j_n(r,\omega) j_m(r',\omega')\rangle &= 4\omega\varepsilon_0\pi\delta(\omega+\omega')\{\mathrm{Im}[\varepsilon_e(r',\omega)]n[T_e(r',t),\omega] \\ &+ \mathrm{Im}[\varepsilon_{lat}(r',\omega)]n[T_{lat}(r',t),\omega]\}\delta(r-r')\end{aligned} \quad (5)$$

where ε_0, ε_e, and ε_{lat} are the permittivity of vacuum, electronic, and phononic systems, respectively, and $n(\omega, T) = \hbar\omega\left(\exp\left(\frac{\hbar\omega}{k_B T}\right) - 1\right)^{-1}$ is the mean energy of Planck's oscillator. In contrast to the typical form of FDT for equilibrium systems,[26,66] (5) is valid when the time scale of interest is shorter than the thermalization time of hot carriers. Notably, this description extends previously established steady-state fluctuational electrodynamics to the time domain. Therefore, we can calculate the near-field radiative heat transfer due to ultrafast hot carrier transport and interaction dynamics. To address potential concerns about the validity of FDT in time-varying systems, we also considered the impact of time-harmonic modulation effects on thermal emission, as introduced by Vázquez-Lozano and Liberal.[67] Our results confirm that time modulation has a significant effect on graphene in the far-field regime, whereas in the near-field, this effect is negligible due to the much stronger enhancement from evanescent waves unrelated to time modulation (see SI).

Due to its small heat capacity, the nanotip region is assumed to be isothermal at 297 K. The high thermal power sensitivity of the proposed technique is achieved by the scanning thermal probe,[21,23] in which a nanothermometer embedded in the tip is thermally insulated from the large thermal reservoir (e.g., the microfabricated chip) via a weak thermal link (e.g., a soft cantilever made of low thermal conductivity materials). To optimize the near-field radiation absorption, large nanotip radius R_{tip} and small gap sizes d between the tip and the sample are favorable. However, R_{tip} sets the lower limit for the spatial resolution of the technique. To enable sufficient spatial resolution to identify nanoscale phonon transport effects in graphene while obtaining a sufficient near-field absorption magnitude, we selected R_{tip} = 100 nm. Even though the tip size is much smaller than the thermal wavelength, a dipole approximation is not applicable in the present many-body near-field radiation scenario because the tip radius is much larger than the gap size ($R_{tip}/d \gg 1$).[68,69] Therefore, without loss of generality, we use the proximity approximation to estimate near-field radiation heat transfer as follows

$$Q^{th} = \int \frac{dA}{(\pi R_{tip}^2 t_{gr})} q^{th}(T, \bar{d}(r)) \quad (6)$$

where dA is the element of area, t_{gr} is the thickness of monolayer graphene, and $\bar{d}(r) = d + R_{tip} - \sqrt{R_{tip}^2 - r^2}$ is the local gap size between the tip and the sample. The flux $q_{e/p}^{th}$ contributed by phonons or electrons is obtained as the near-field between two semi-infinite plates

$$q_{e/p}^{th} = \sum_{e,p} \frac{1}{4\pi^2} \int_0^\infty d\omega[n(\omega, T_{e/p}) - n(\omega, T_{tip})] \times \int_0^\infty \Gamma(\omega, k) k dk \quad (7)$$

where k is the component of the wavevector parallel to the sample's surface, and Γ is the transmission coefficient for both the propagating and evanescent waves. The contribution of the p-polarized evanescent wave dominates in the near-field,[25,26,66] as described by

$$\Gamma = \frac{4\mathrm{Im}(R_1^p)\mathrm{Im}(R_3^p)e^{-2\mathrm{Im}(\gamma_2)\bar{d}}}{|1 - R_1^p R_3^p e^{i2\gamma_2\bar{d}}|^2} \quad (8)$$

where γ_2 is the perpendicular wavevector with respect to medium 2 (vacuum gap), and R_1, R_3 are reflection coefficients from the vacuum medium to thin-film medium 1 (graphene) and to medium 3 (tip). A detailed description of this calculation and the required optical properties is provided in the Supporting Information.

We employ a model following ref 70 to calculate the near-field thermal signal that is scattered into the far field by a nanotip that is brought into the evanescent field of the sample. We assume a nonlocal, temperature-dependent dielectric function of monolayer graphene that has been experimentally confirmed in recent near-field optical microscopy experiments.[71,72] Unlike the traditional image-dipole model, which has limited applicability, "dressed" polarizabilities are used to account for multiple reflections between the probe and the surface. As detailed in the Supporting Information, the scattered power can be calculated as follows

$$Q_{e/p}^{S} = \frac{\mu_0\omega^4 d\Omega}{32\pi^2 c} \sum_{i,j,k} \left(\Gamma_{ij}^{E}\alpha_{ij}^{EE}E_j^0 + \frac{1}{c}\Gamma_{ij}^{H}\beta_{ij}^{HH}H_j^0\right) \times \left(\Gamma_{ik}^{E*}\alpha_{kk}^{EE*}E_k^{0*} + \frac{1}{c}\Gamma_{ik}^{H*}\beta_{kk}^{HH*}H_k^{0*}\right) \quad (9)$$

where μ_0 is the permeability of vacuum, $d\Omega$ denotes the solid angle that the detector subtends, c is the speed of light, α^{EE} and β^{HH} are the electric and magnetic dressed polarizabilities, respectively, and E^0 and H^0 are the local electric and magnetic fields at the tip. Tensors Γ^E and Γ^H characterize multiple reflections between the tip and sample and account for interference patterns between emitted and reflected rays.[70] Superscript * denotes the complex conjugate. As detailed in the Supporting Information, the previous expression simplifies and can be numerically evaluated by assuming that the electric and magnetic fields solely originate from thermal emission.

We use temperature-dependent optical properties for both electrons and the lattice in graphene. For the former, we consider the Lindhard model to account for nonlocal electronic conductivity.[73−76] For the latter, we use the Lorentz model.[46] Details on the implementation of these models and the optical properties can be found in the Supporting Information. In the following case studies, we have chosen monolayer graphene as the example material due to its extensively studied hot carrier effects and high extrinsic tunability for experimental validations. However, note that our model is valid and can be generalized to other materials beyond graphene. Specifically, the assumptions applied to graphene regarding hot electron and phonon transport are generally applicable to the broad class of two-dimensional (2D) electron and hole gas materials (2DEG/2DHG) such as other 2D materials and their heterostructures, semiconductor interfaces based on silicon or III−V compounds, and the interfaces of some insulating oxides. Furthermore, we use the nanotip-based configuration as shown in Figure 1 because

https://doi.org/10.1021/acsnano.4c11893
ACS Nano 2025, 19, 6033−6043

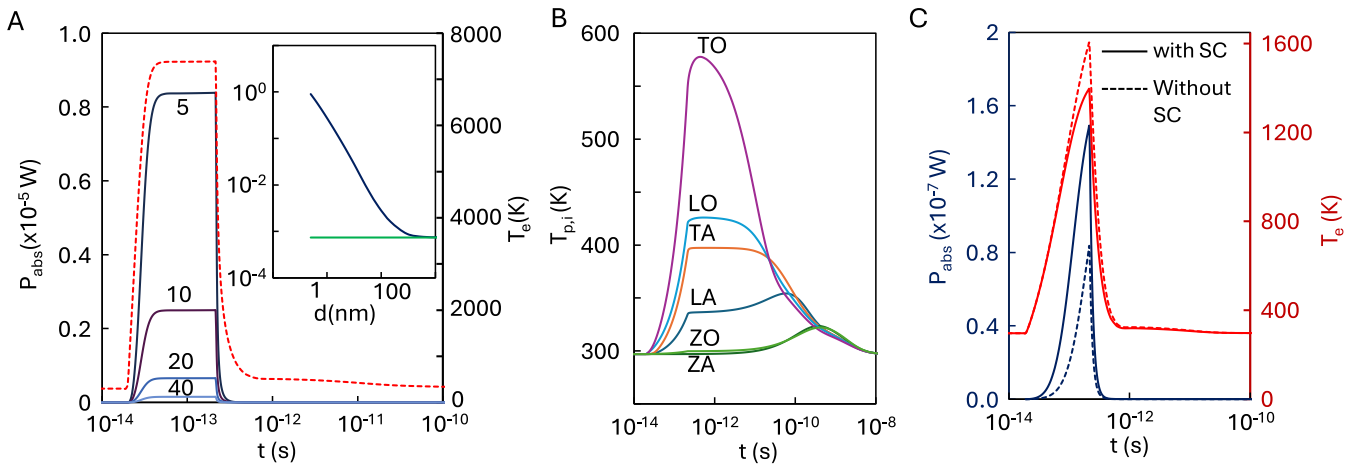

Figure 2. (A) Hot electron temperature (dashed line) and near-field power for μ = 0.25 eV and gap sizes of d = 5, 10, 20, and 40 nm (solid lines) at the center of the excitation for a pump spot size of L = 400 nm. The inset shows the maximum near-field (blue) and far-field (green) power as a function of the gap size. (B) Dynamics of different hot phonon branches for the laser excitation in (A). (C) Effect of electron supercollision on the hot electron temperature (red) and near-field radiation (blue) for d = 5 nm. The case including supercollisions with μ = 0.25 eV (solid lines), and the case without supercollisions with μ = 1.4 eV (dash lines) are shown for the same spot size and a laser power 50 times smaller than in (A, B).

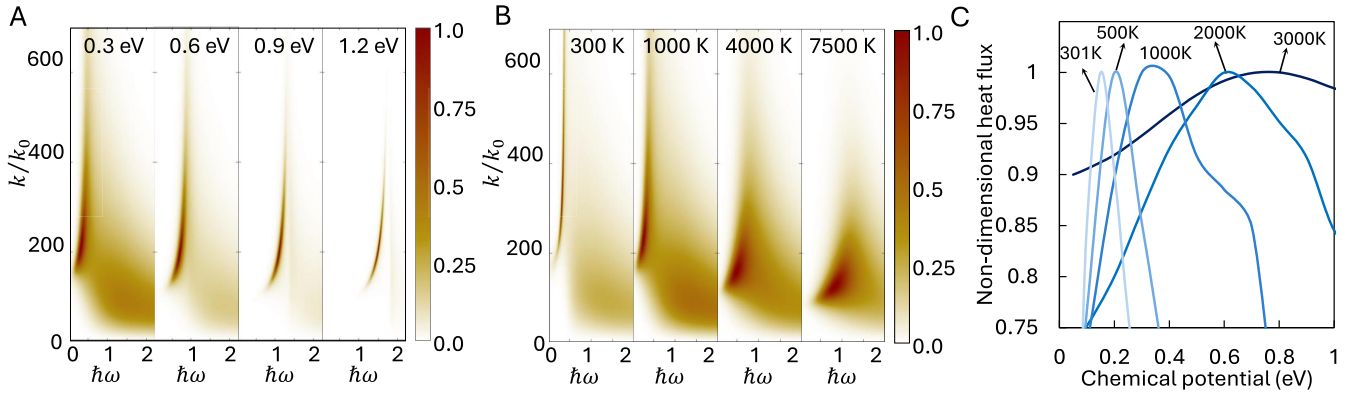

Figure 3. (A) Transmission coefficients Γ for different μ values at T_e = 1000 K. (B) Γ for different T_e values with μ = 0.25 eV. (C) Effect of chemical potential and hot electron temperature on near-field radiative heat flux.

among the three main configurations of near-field thermal radiation—nanotip-plate, microsphere-plate, and parallel plate—plate, the nanotip configuration is the one that achieves nanometer-scale spatial resolution as shown in previous work[18,19] and thus enables direct probing of nanoscale hot carrier transport and nonequilibrium behaviors.

Electron Supercollision Effect. In response to ultrafast laser excitation, the model predicts hot electron dynamics and associated near-field radiation as illustrated in Figure 2A. Hot electrons exhibit a giant increase in their temperature upon optical excitation, which is much stronger and faster than that of the phonon branches (Figure 2B). This can be attributed to both the major laser absorption by electrons (~90%) and their small heat capacity. Consequently, a remarkable thermal switching behavior in near-field radiative heat transfer occurs at ps scale.[34,77] In contrast, the contribution of phonons to near-field radiation is marginal, leading to a rapid drop in the near-field flux shortly after the optical excitation is turned off. Hot electrons relax by transferring energy to the lattice via different el–ph scattering mechanisms, thus exciting different phonon branches to distinct temperatures depending on the coupling strength and the phonon-specific heat capacity (Figure 2B). Subsequently and until the system reaches global equilibrium, the electron and lattice temperatures remain equilibrated allowing the tracking of the phonon evolution by measuring the near-field flux radiated by electrons. Throughout the process, near-field radiation is extremely sensitive to the gap size d, resulting in ~3 to 4 orders of magnitude enhancement in the extreme near-field (d less than 10 nm) relative to the far field. The minimum gap size of 5 nm chosen in our calculations is motivated by previous near-field thermal radiation experiments[21,23] and theoretical calculations[36−38] in the extreme near field, which have shown that non-near-field heat transfer between sample and tip and the interplay between near-field thermal radiation and conduction within the tip are negligible in this regime. Furthermore, the minimal gap size is also chosen because the interaction between the laser excitation and the tip may exhibit plasmonic strong-coupling effects within nanogaps smaller than 1–2 nm, as show in recent experiments.[78,79] These effects may invalidate the near-field thermal radiation model implemented in this work.

Hot electron dynamics and near-field thermal behavior can be controlled in monolayer graphene by tuning the chemical potential, which strongly affects the nonlinear el–ph (acoustic) supercollision effect. This can be achieved, for example, by engineering the abundance of defects in graphene. In Figure

https://doi.org/10.1021/acsnano.4c11893
ACS Nano 2025, 19, 6033−6043

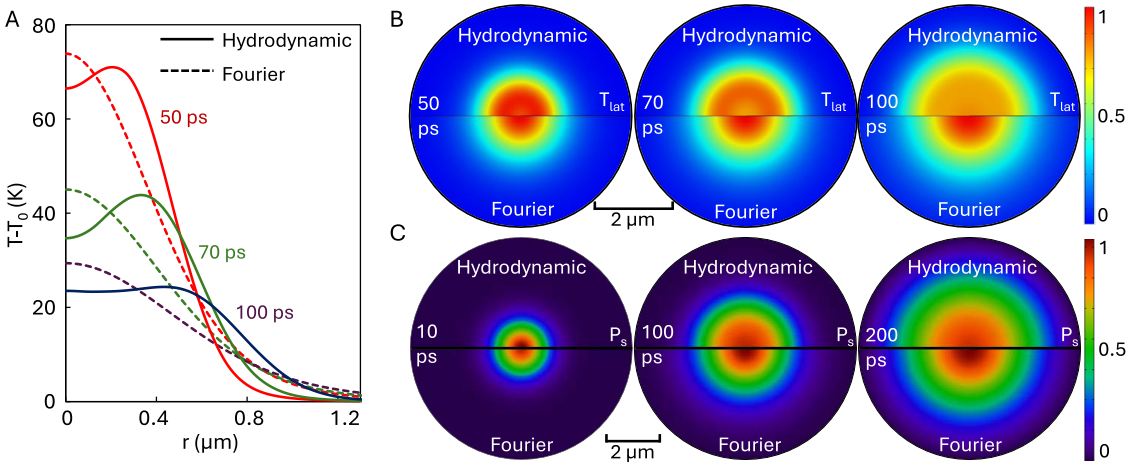

Figure 4. (A) Radial profile of lattice temperature for hydrodynamic (solid) and Fourier (dashed) model, (B) distribution of normalized T_{lat}, and (C) nanoscale mapping of scattered near-field thermal radiation by the scanning probe with gap size d = 5 nm at different sampling times for a pump spot size L = 200 nm and a laser power 20 times higher than in Figure 2A,B. The hydrodynamic model prediction does not include non-local viscous effects.

2C, we compare the near-field heat flux for two cases, μ = 0.25 and μ = 1.4 eV, for which the range of electron temperatures wherein supercollision becomes pronounced is found to be T_e > 290 and T_e > 1625 K, respectively. Thus, by reducing the laser power so that T_e is lower than 1600 K, only the lower μ case displays supercollision effects. Provided the low temperatures of acoustic phonons, we find more efficient cooling of hot electrons in the presence of supercollision. However, although the hot electron temperature for μ = 0.25 eV is lower than that for μ = 1.4 eV, the near-field heat flux is surprisingly higher. This is due to the competing effects of chemical potential and hot electron temperature on near-field thermal radiation as discussed below. The clearly demonstrated differences between linear hot electron cooling mechanisms and nonlinear supercooling in Figure 2 are of great interest to be probed by near-field hot carrier nanoscopy. In fact, significant debates still exist regarding the role and relative strength of different linear and nonlinear electron cooling pathways, which are strongly dependent on nanoscale features such as defects and disorder and the complicated interplay between local electronic structure, chemical potential, and hot electron temperature. Past theoretical and experimental works[80−85] have been mostly focused on phenomenological and macroscopic understanding or have used far-field optics or bulk-scale electrical characterization methods that do not provide enough resolution to distinguish nanoscale effects. In contrast, our model shows that near-field thermal radiation imaging with high spatial and temporal resolution can provide a means to distinguish different nonequilibrium hot electron cooling mechanisms.

The spectral- and mode-resolved near-field energy transmission is shown in Figure 3A,3B. Notably, the dispersion relation for graphene,[86] $\frac{\varepsilon_1}{\gamma_1} + \frac{\varepsilon_2}{\gamma_2} = -4\pi\left(\frac{c}{\omega}\right)\alpha\sigma(\mu, T)$, where α is the fine structure constant, depends on both μ and T_e via the electrical conductivity σ. In consequence, surface plasmon polaritons (SPPs) can be modulated by varying the magnitudes of either parameter. A reduction in μ amplifies the intensity of the SPPs, leading to stronger near-field thermal radiation (Figure 3A). Moreover, hotter electrons lead to a smaller contributing number of modes of SPPs for $k > 200k_0$ (Figure 3B). Due to these competing effects, for a given hot electron temperature, an optimal chemical potential for near-field heat flux exists (see Figure 3C). For the temperature range in this study, μ = 0.25 eV provides the optimal near-field thermal radiation characteristics in graphene, and hence, this particular chemical potential value is assumed for the discussion below.

Hydrodynamic Phonon Transport: Second Sound. We proceed to study two hydrodynamic phonon transport effects: second sound, which refers to the propagation of a thermal wave through the lattice due to phonon memory effects, and thermal viscosity due to nonlocal phonon transport. The emergence, coexistence, and interplay of these effects are poorly understood so far and are subjects of ongoing debate. One school of thought suggests that at high temperatures (e.g., room temperature), the evolution of different phonon modes is uncorrelated due to the dominance of resistive scattering over momentum-conserving scattering, preventing the manifestation of collective phonon dynamics and hydrodynamic effects. In contrast, it has long been proposed that these effects should generally be observed at the nanoscale even at high temperatures due to the slow and collective relaxation of the heat flux.[87] Previous works reporting the observation of second sound[62,63,88−90] or the nonlocal decoupling of the thermal gradient and the heat flux[91−94] are insufficient to clarify the origin and minimal conditions for the emergence of hydrodynamic phonon transport. To address this debate, near-field thermal imaging enables the resolution of the nondiffusive transport features that distinguish phonon hydrodynamics at the nanoscale from alternative interpretations based on the independent evolution of different phonon modes.

We first neglect nonlocal effects in our calculations to isolate the influence of heat inertia by assuming l_i = 0 in eq 4.[35] This situation has been identified in experiments involving extremely small excitation length scales.[62] The main signature of memory effects in the present conditions is a wavefront in the lattice temperature field, which can be measured indirectly by monitoring the hot electron temperature and near-field thermal radiation. At time scales similar to the phonon scattering time, energy propagates as a damped thermal pulse initiating at ∼40 ps and culminating at ∼300 ps (Figure 4A). Since we are considering ultrafast time scales wherein the different branches are not in equilibrium, a different character-

https://doi.org/10.1021/acsnano.4c11893
ACS Nano 2025, 19, 6033−6043

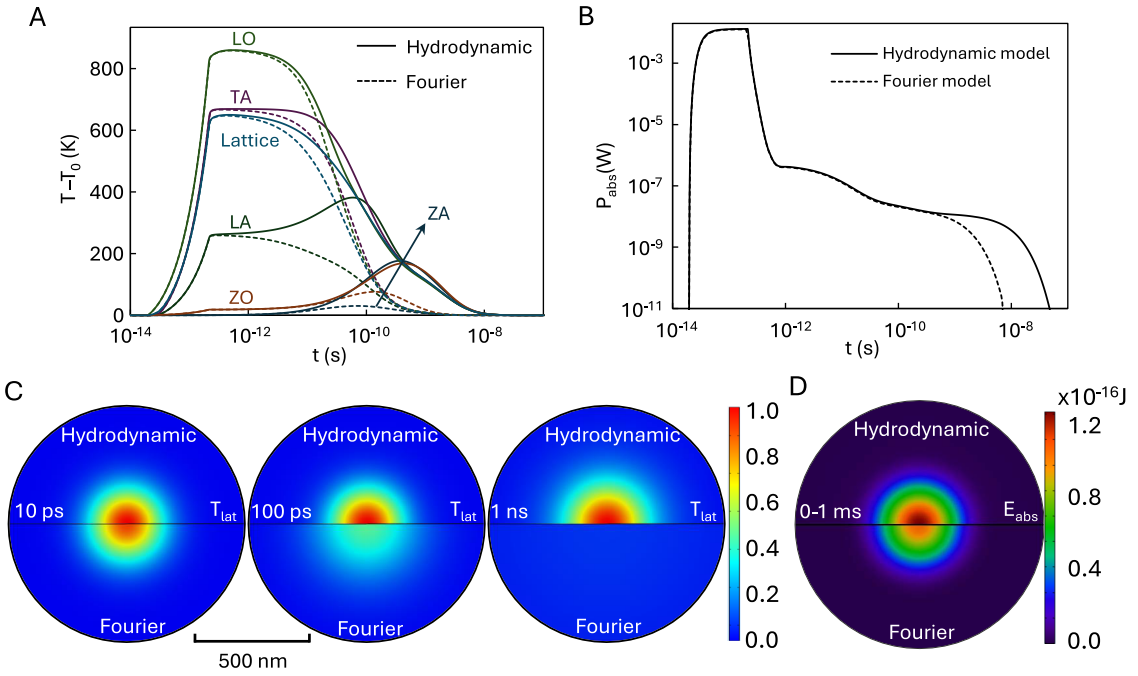

Figure 5. (A) Phonon temperatures and (B) near-field flux at the center of the excitation according to Fourier (dashed) and full hydrodynamic (solid) models. (C) Distribution of normalized T_{lat} at different sampling times. (D) Nanoscale mapping of absorbed near-field radiation by the scanning probe with gap size d = 5 nm during the first 1 ms after excitation for a pump spot size L = 400 nm and a laser power 20 times higher than in Figure 2A,2B.

istic pulse velocity, $\sim\sqrt{\frac{\kappa_{p_i}}{C_{p_i}\tau_{p_i}}}$, can be identified for each branch. Nonetheless, the thermal wave also manifests in the lattice thermal field with an average velocity (i.e., the second sound velocity). In contrast to the Fourier model predictions ($\tau_i = l_i = 0$), the finite wave velocity thus bounds the expansion of the perturbed region and significantly modifies the pattern observed in the near-field heat flux mapping. In addition, the temperature and near-field scattering power in the central point diminish faster as a consequence of the efficient energy dissipation enhanced by the thermal wave. These nondiffusive signatures are evident by comparing the temperature map and the resulting scattered light by the nanotip across the sample at different sampling times, as shown in Figure 4B,4C, respectively. Interestingly, since the imaging presented here is based on a noncontact technique, the measurements are insensitive to elastic wave propagation (first sound), which facilitates unambiguous identification of wave-like effects on the temperature field. Furthermore, we note that (1) and (2) can be easily coupled with linear elastic equations to investigate thermoelastic effects that might emerge under the extreme nonequilibrium conditions considered here.

Hydrodynamic Phonon Transport: Nonlocal Effect. According to eq 4, however, second sound is not the only nondiffusive transport behavior potentially emerging at the nanoscale. In the presence of inhomogeneous energy flux distributions, viscous effects can reduce the thermal energy transferred for a given temperature gradient. The lack of resistive ph−ph scattering within regions smaller than the average MFP precludes the homogenization of the flux and temperature profiles and leads to fluid-like behavior such as heat vorticity. In experiments, these effects are usually interpreted as a ballistic reduction of the apparent thermal conductivity[91] and never observed coexisting with the second sound. Here, we illustrate the nonlocal transient effects and their influence on the observable near-field thermal radiation by considering the full hydrodynamic model ($l_i \neq 0$ and $\tau_i \neq 0$). Nonlocality manifests as a slowly evolving lattice temperature distribution relative to the diffusive prediction (Figure 5A), which contributes to less effective cooling of hot electrons. Hence, the signature of nonlocal phonon transport can be detected as a delayed decay in near-field heat flux absorbed by the nanotip, which extends to over 10 ns after the ultrashort optical excitation (Figure 5B). This can potentially be measured experimentally through the nanoscale lattice (phononic) temperature map (Figure 5C) by imaging the near-field heat flux (Figure 5D). Note that a scanning thermal probe can be used to measure the total thermal absorption (integrated over 1 ms in Figure 5D), similar to the detection of a short infrared pulse in a bolometer device. The calculated total absorption of the near-field thermal signal, on the scale of sub-fJ, can be readily detected by current picowatt, sub-ms resolution thermal probes.[95] Furthermore, relevant to practical applications typically under continuous or low-frequency electrical excitations, the manifestation of nonlocal effects on phonon transport can also be investigated in these static or near-static conditions using the present hot carrier nanoscopy technique. In the Supporting Information, we show example applications considering electrical excitation in a monolayer graphene and gallium arsenide with nanoscale constrictions, where the near-field thermal absorption flux and local lattice temperature can be simultaneously resolved through high-resolution contact- and noncontact mode hot carrier nanoscopy.

The non-Fourier predictions in Figures 4 and 5 are qualitatively different. This emphasizes the suitability of these experiments for distinguishing the interplay between diffusion and the different hydrodynamic effects predicted by the present theoretical framework. Furthermore, the persistent

https://doi.org/10.1021/acsnano.4c11893
ACS Nano 2025, 19, 6033−6043

heterogeneity of the temperature distribution due to nonlocal transport in Figure 5 is strongly dependent on the relation between the nonlocal length of the dominant phonon branches and the focused laser spot size, L = 400 nm (see Supporting Information). Investigating the onset of the non-Fourier signatures as a function of L is thus a promising approach for comparing the present hydrodynamic description with alternative multiscale theories such as the ballistic phonon mode suppression[11] or the truncated Lèvy flight formalism,[96,97] where the emergence of nondiffusive effects is predicted at much larger length scales comparable to the largest phonon means free paths.

The present model has been developed as a predictive tool for length and time scales comparable to those of the phonon−electron and phonon−phonon interactions in monolayer graphene. At even smaller time and length scales, however, a fully ballistic limit for phonons is reached, which is beyond the validity of the hydrodynamic model based on integrated magnitudes such as heat fluxes and temperatures.[41] Moreover, the use of a unique local-equilibrium temperature for electrons is inadequate at length and time scales comparable to or smaller than the electron thermalization process via electron−electron interactions. Furthermore, nondiffusive electron transport signatures can be significant in ultraclean samples at smaller scales or cryogenic temperatures, which would require generalizing the electronic heat flux constitutive relation in eq 3.[55,98] Finally, for complex materials displaying anisotropic dispersion relations, generalization of the transport equations is required by introducing the notion of anisotropic viscosity tensors.[99]

CONCLUSIONS

We presented a comprehensive quantitative model accounting for the near-field thermal radiation signatures of microscopic energy transport processes in low-dimensional materials such as graphene and 2D electron gas systems in general. We proposed a tool, near-field hot carrier nanoscopy, that can be leveraged to detect and differentiate between different hot electron and hot phonon transport phenomena based on the measured near-field thermal absorption and scattering signal from a scanning nanotip. This method offers intrinsically high spatial and temporal resolution when combined with highly sensitive scanning thermal microscopy probes and ultrafast spectroscopy, addressing the existing limitations of far-field hot carrier characterization techniques. Thus, this model directly links various hot carrier effects to experimentally measurable near-field thermal signals. Specifically, we predict sub-picosecond level ultrafast radiative heat transfer due to hot electron absorption and show that nonlinear electron−phonon interactions can enhance or suppress near-field thermal radiation, depending on the competing effects of chemical potential and electron temperature. Further, we provide insight into distinguishing between second sound and heat viscosity using nanoscale near-field probing. We anticipate that our model will serve as a theoretical foundation to inform future experiments to map nondiffusive transport and addressing ongoing debates on the emergence and competing roles of different hydrodynamic effects.

METHODS

A time-domain fluctuational electrodynamic model is used in this work to describe the near-field thermal absorption and scattering by a nanotip induced by ultrafast hot electron and phonon transport and interactions in optically excited monolayer graphene (see SI). Linear and nonlinear hot carrier transport effects including electron supercollision, phonon memory, and nonlocal phonon transport are incorporated into a generalized multitemperature model to obtain the temperatures of hot electrons and phonons, as well as the heat flux under diffusive and hydrodynamic transport regimes. The model equations are solved using the Galerkin method, implemented in the finite element solver COMSOL Multiphysics.[64]

ASSOCIATED CONTENT

Supporting Information

The Supporting Information is available free of charge at https://pubs.acs.org/doi/10.1021/acsnano.4c11893.

> Near-field radiative heat transfer model, scattered near-field radiation, optical properties of hot carriers in graphene, selection of the nanotip material, sensitivity and resolution requirements of near-field hot carrier nanoscopy, effect of laser pulse duration, effect of laser spot size, and near-field hot carrier nanoscopy for steady-state nonlocal phonon transport probing (PDF)

AUTHOR INFORMATION

Corresponding Author

Longji Cui − *Department of Mechanical Engineering, University of Colorado Boulder, Boulder, Colorado 80309, United States; Materials Science and Engineering Program and Center for Experiments on Quantum Materials, University of Colorado Boulder, Boulder, Colorado 80309, United States;* orcid.org/0000-0003-0469-3230; Email: Longji.cui@colorado.edu

Authors

Mohammad Habibi − *Department of Mechanical Engineering, University of Colorado Boulder, Boulder, Colorado 80309, United States*

Albert Beardo − *Department of Physics, JILA, and STROBE NSF Science and Technology Center, University of Colorado and NIST, Boulder, Colorado 80309, United States*

Complete contact information is available at: https://pubs.acs.org/10.1021/acsnano.4c11893

Funding

A.B. acknowledges support from the STROBE National Science Foundation Science & Technology Center, Grant No. DMR-1548924, and from the Spanish Ministry of Universities through a Margarita Salas fellowship funded by the European Union—NextGenerationEU.

Funding

This work is supported by NSF (CAREER CBET-2239004) and AFRL (FA8651-22-1-0012). This work utilized resources from the University of Colorado Boulder Research Computing, which is supported by NSF (ACI-1532235 and ACI-1532236), the University of Colorado Boulder, and Colorado State University.

Notes

The authors declare no competing financial interest.

ACKNOWLEDGMENTS

We acknowledge Pramod Reddy, Xiulin Ruan, Henry Kapteyn, and Margaret Murnane for helpful discussions.

ABBREVIATIONS

MFP mean free path
FDT fluctuation−dissipation theorem
LDOS local density of states
SPPs surface plasmon polaritons

REFERENCES

(1) Reggiani, L. *Hot-Electron Transport in Semiconductors*; Springer Science & Business Media, 2006.
(2) Paul, K. K.; Kim, J.-H.; Lee, Y. H. Hot carrier photovoltaics in van der Waals heterostructures. *Nat. Rev. Phys.* **2021**, *3*, 178−192.
(3) Cui, L.; Zhu, Y.; Abbasi, M.; Ahmadivand, A.; Gerislioglu, B.; Nordlander, P.; Natelson, D. Electrically Driven Hot-Carrier Generation and Above-Threshold Light Emission in Plasmonic Tunnel Junctions. *Nano Lett.* **2020**, *20*, 6067−6075.
(4) Gabor, N. M.; Song, J. C. W.; Ma, Q.; Nair, N. L.; Taychatanapat, T.; Watanabe, K.; Taniguchi, T.; Levitov, L. S.; Jarillo-Herrero, P. Hot Carrier-Assisted Intrinsic Photoresponse in Graphene. *Science* **2011**, *334*, 648−652.
(5) Cai, X.; Sushkov, A. B.; Suess, R. J.; Jadidi, M. M.; Jenkins, G. S.; Nyakiti, L. O.; Myers-Ward, R. L.; Li, S.; Yan, J.; Gaskill, D. K.; Murphy, T. E.; Drew, H. D.; Fuhrer, M. S. Sensitive room-temperature terahertz detection via the photothermoelectric effect in graphene. *Nat. Nanotechnol.* **2014**, *9*, 814−819.
(6) Cortés, E.; Besteiro, L. V.; Alabastri, A.; Baldi, A.; Tagliabue, G.; Demetriadou, A.; Narang, P. Challenges in Plasmonic Catalysis. *ACS Nano* **2020**, *14*, 16202−16219.
(7) Chen, Z.; Sjakste, J.; Dong, J.; Taleb-Ibrahimi, A.; Rueff, J.-P.; Shukla, A.; et al. Ultrafast dynamics of hot carriers in a quasi−two−dimensional electron gas on InSe. *Proc. Natl. Acad. Sci. U.S.A.* **2020**, *117*, 21962−21967.
(8) Zhang, Y.; Shi, X.; You, W.; Tao, Z.; Zhong, Y.; Kabeer, F. C.; et al. Coherent modulation of the electron temperature and electron−phonon couplings in a 2D material. *Proc. Natl. Acad. Sci. U.S.A.* **2020**, *117*, 8788−8793.
(9) Shi, X.; You, W.; Zhang, Y.; Tao, Z.; Oppeneer, P. M.; Wu, X.; Thomale, R.; Rossnagel, K.; Bauer, M.; Kapteyn, H.; Murnane, M. Ultrafast electron calorimetry uncovers a new long-lived metastable state in mediated by mode-selective electron-phonon coupling. *Sci. Adv.* **2019**, *5*, No. eaav4449.
(10) Wilson, R. B.; Cahill, D. G. Anisotropic failure of Fourier theory in time-domain thermoreflectance experiments. *Nat. Commun.* **2014**, *5*, 5075.
(11) Hu, Y.; Zeng, L.; Minnich, A. J.; Dresselhaus, M. S.; Chen, G. Spectral mapping of thermal conductivity through nanoscale ballistic transport. *Nat. Nanotechnol.* **2015**, *10*, 701−706.
(12) Ziabari, A.; Torres, P.; Vermeersch, B.; Xuan, Y.; Cartoixà, X.; Torelló, A.; et al. Full-field thermal imaging of quasiballistic crosstalk reduction in nanoscale devices. *Nat. Commun.* **2018**, *9*, No. 255.
(13) Najafi, E.; Ivanov, V.; Zewail, A.; Bernardi, M. Super-diffusion of excited carriers in semiconductors. *Nat. Commun.* **2017**, *8*, No. 15177.
(14) Guyer, R. A.; Krumhansl, J. A. Thermal Conductivity, Second Sound, and Phonon Hydrodynamic Phenomena in Nonmetallic Crystals. *Phys. Rev.* **1966**, *148*, 778−788.
(15) Sendra, L.; Beardo, A.; Bafaluy, J.; Torres, P.; Alvarez, F. X.; Camacho, J. Hydrodynamic heat transport in dielectric crystals in the collective limit and the drifting/driftless velocity conundrum. *Phys. Rev. B* **2022**, *106*, No. 155301.
(16) Shang, M.-Y.; Mao, W.-H.; Yang, N.; Li, B.; Lü, J.-T. Unified theory of second sound in two-dimensional materials. *Phys. Rev. B* **2022**, *105*, No. 165423.
(17) Hua, C.; Lindsay, L.; Chen, X.; Minnich, A. J. Generalized Fourier's law for nondiffusive thermal transport: Theory and experiment. *Phys. Rev. B* **2019**, *100*, No. 085203.
(18) Weng, S. K. Q.; Yang, L.; An, Z.; Chen, P.; Biehs, S.-A.; Kajihara, Y.; Lu, W. Imaging of nonlocal hot-electron energy dissipation via shot noise. *Science* **2018**, *360*, 775−778.
(19) De Wilde, Y.; Formanek, F.; Carminati, R.; Gralak, B.; Lemoine, P.-A.; Joulain, K.; Mulet, J.-P.; Chen, Y.; Greffet, J.-J. Thermal radiation scanning tunnelling microscopy. *Nature* **2006**, *444*, 740−743.
(20) Jones, A. C.; Raschke, M. B. Thermal Infrared Near-Field Spectroscopy. *Nano Lett.* **2012**, *12*, 1475−1481.
(21) Kim, K.; Song, B.; Fernàndez-Hurtado, V.; Lee, W.; Jeong, W.; Cui, L.; et al. Radiative heat transfer in the extreme near field. *Nature* **2015**, *528*, 387−391.
(22) Menges, F.; Riel, H.; Stemmer, A.; Gotsmann, B. Quantitative Thermometry of Nanoscale Hot Spots. *Nano Lett.* **2012**, *12*, 596−601.
(23) Cui, L.; Jeong, W.; Fernàndez-Hurtado, V.; Feist, J.; García-Vidal, F. J.; Cuevas, J. C.; Meyhofer, E.; Reddy, P. Study of radiative heat transfer in Ångström- and nanometre-sized gaps. *Nat. Commun.* **2017**, *8*, No. 14479.
(24) Cui, L.; Jeong, W.; Hur, S.; Matt, M.; Klöckner, J. C.; Pauly, F.; Nielaba, P.; Cuevas, J. C.; Meyhofer, E.; Reddy, P. Quantized thermal transport in single-atom junctions. *Science* **2017**, *355*, 1192−1195.
(25) Polder, D.; Van Hove, M. Theory of Radiative Heat Transfer between Closely Spaced Bodies. *Phys. Rev. B* **1971**, *4*, 3303−3314.
(26) Joulain, K.; Mulet, J.-P.; Marquier, F.; Carminati, R.; Greffet, J.-J. Surface electromagnetic waves thermally excited: Radiative heat transfer, coherence properties and Casimir forces revisited in the near field. *Surf. Sci. Rep.* **2005**, *57*, 59−112.
(27) Sheng, A. N.; Chen, G. Surface Phonon Polaritons Mediated Energy Transfer between Nanoscale Gaps. *Nano Lett.* **2009**, *9*, 2909−2913.
(28) Basu, S.; Zhang, Z. M.; Fu, C. J. Review of near-field thermal radiation and its application to energy conversion. *Int. J. Energy Res.* **2009**, *33*, 1203−1232.
(29) Yang, Y.; Wang, L. Spectrally Enhancing Near-Field Radiative Transfer between Metallic Gratings by Exciting Magnetic Polaritons in Nanometric Vacuum Gaps. *Phys. Rev. Lett.* **2016**, *117*, No. 044301.
(30) Zhu, L.; Fan, S. Persistent Directional Current at Equilibrium in Nonreciprocal Many-Body Near Field Electromagnetic Heat Transfer. *Phys. Rev. Lett.* **2016**, *117*, No. 134303.
(31) Lim, M.; Song, J.; Lee, S. S.; Lee, B. J. Tailoring near-field thermal radiation between metallo-dielectric multilayers using coupled surface plasmon polaritons. *Nat. Commun.* **2018**, *9*, 4302.
(32) Biehs, S. A.; Messina, R.; Venkataram, P. S.; Rodriguez, A. W.; Cuevas, J. C.; Ben-Abdallah, P. Near-field radiative heat transfer in many-body systems. *Rev. Mod. Phys.* **2021**, *93*, No. 025009.
(33) Wu, H.; Liu, X.; Cai, Y.; Cui, L.; Huang, Y. Near-field radiative heat transfer modulated by nontrivial topological surface states. *Mater. Today Phys.* **2022**, *27*, No. 100825.
(34) Yu, R.; Manjavacas, A.; García de Abajo, F. J. Ultrafast radiative heat transfer. *Nat. Commun.* **2017**, *8*, No. 2.
(35) Becerril, D.; Camacho de la Rosa, A.; Esquivel-Sirvent, R. Transient effects in the coupling of thermal radiation and non-Fourier heat transport at the nano-scale. *J. Appl. Phys.* **2023**, *134*, No. 084301.
(36) Reina, M.; Messina, R.; Ben-Abdallah, P. Conduction-radiation coupling between two closely separated solids. *Phys. Rev. Lett.* **2020**, *125*, No. 224302.
(37) Wong, B. T.; Francoeur, M.; Bong, V. N.-S.; Mengüç, M. P. Coupling of near-field thermal radiative heating and phonon Monte Carlo simulation: Assessment of temperature gradient in n-doped silicon thin film. *J. Quant. Spectrosc. Radiat. Transfer* **2014**, *143*, 46−55. Special Issue: The Seventh International Symposium on Radiative Transfer.
(38) Messina, R.; Tschikin, M.; Biehs, S.-A.; Ben-Abdallah, P. Fluctuation-electrodynamic theory and dynamics of heat transfer in systems of multiple dipoles. *Phys. Rev. B* **2013**, *88*, No. 104307.
(39) Laitinen, A.; Oksanen, M.; Fay, A.; Cox, D.; Tomi, M.; Virtanen, P.; Hakonen, P. J. Electron-Phonon Coupling in Suspended Graphene: Supercollisions by Ripples. *Nano Lett.* **2014**, *14*, 3009−3013.

https://doi.org/10.1021/acsnano.4c11893
ACS Nano 2025, 19, 6033−6043

(40) Song, J. C. W.; Reizer, M. Y.; Levitov, L. S. Disorder-Assisted Electron-Phonon Scattering and Cooling Pathways in Graphene. *Phys. Rev. Lett.* **2012**, *109*, No. 106602.
(41) Sendra, L.; Beardo, A.; Torres, P.; Bafaluy, J.; Alvarez, F. X.; Camacho, J. Derivation of a hydrodynamic heat equation from the phonon Boltzmann equation for general semiconductors. *Phys. Rev. B* **2021**, *103*, No. L140301.
(42) Lee, S.; Broido, D.; Esfarjani, K.; Chen, G. Hydrodynamic phonon transport in suspended graphene. *Nat. Commun.* **2015**, *6*, 6290.
(43) Cepellotti, A.; Fugallo, G.; Paulatto, L.; Lazzeri, M.; Mauri, F.; Marzari, N. Phonon hydrodynamics in two-dimensional materials. *Nat. Commun.* **2015**, *6*, 6400.
(44) Anisimov, S. I.; Perel'man, T. L. Electron emission from metal surfaces exposed to ultrashort laser pulses. *Zh. Eksp. Teor. Fiz.* **1974**, *66*, No. 076403.
(45) Lu, Z.; Vallabhaneni, A.; Cao, B.; Ruan, X. Phonon branch-resolved electron-phonon coupling and the multitemperature model. *Phys. Rev. B* **2018**, *98*, No. 134309.
(46) Ochoa-Martínez, E.; Gabàs, M.; Barrutia, L.; Pesquera, A.; Centeno, A.; Palanco, S.; Zurutuza, A.; Algora, C. Determination of a refractive index and an extinction coefficient of standard production of CVD-graphene. *Nanoscale* **2015**, *7*, 1491−1500.
(47) Song, B.; Gu, H.; Zhu, S.; Jiang, H.; Chen, X.; Zhang, C.; Liu, S. Broadband optical properties of graphene and HOPG investigated by spectroscopic Mueller matrix ellipsometry. *Appl. Surf. Sci.* **2018**, *439*, 1079−1087, DOI: 10.1016/j.apsusc.2018.01.051.
(48) Nair, R. R.; Blake, P.; Grigorenko, A. N.; Novoselov, K. S.; Booth, T. J.; Stauber, T.; Peres, N. M.; Geim, A. K. Fine structure constant defines visual transparency of graphene. *Science* **2008**, *320*, 1308.
(49) Berciaud, S.; Han, M. Y.; Mak, K. F.; Brus, L. E.; Kim, P.; Heinz, T. F. Electron and Optical Phonon Temperatures in Electrically Biased Graphene. *Phys. Rev. Lett.* **2010**, *104*, No. 227401.
(50) Rana, F.; George, P. A.; Strait, J. H.; Dawlaty, J.; Shivaraman, S.; Chandrashekhar, M.; Spencer, M. G. Carrier recombination and generation rates for intravalley and intervalley phonon scattering in graphene. *Phys. Rev. B* **2009**, *79*, No. 115447.
(51) Winzer, T.; Malić, E. Impact of Auger processes on carrier dynamics in graphene. *Phys. Rev. B* **2012**, *85*, No. 241404.
(52) Han, Z.; Sokalski, P.; Shi, L.; Ruan, X. Prediction of hot zone-center optical phonons in laser-irradiated molybdenum disulfide with a semiconductor multitemperature model. *Phys. Rev. B* **2023**, *107*, No. L041407.
(53) Giannazzo, F.; Sonde, S.; Nigro, R. L.; Rimini, E.; Raineri, V. Mapping the Density of Scattering Centers Limiting the Electron Mean Free Path in Graphene. *Nano Lett.* **2011**, *11*, 4612−4618.
(54) Bolotin, K. I.; Sikes, K. J.; Hone, J.; Stormer, H. L.; Kim, P. Temperature-Dependent Transport in Suspended Graphene. *Phys. Rev. Lett.* **2008**, *101*, No. 096802.
(55) Varnavides, G.; Yacoby, A.; Felser, C.; Narang, P. Charge transport and hydrodynamics in materials. *Nat. Rev. Mater.* **2023**, *8*, 726−741.
(56) Scott, R. J.; Valencia-Acuna, P.; Zhao, H. Spatiotemporal Observation of Quasi-Ballistic Transport of Electrons in Graphene. *ACS Nano* **2023**, *17*, 25368−25376.
(57) Young, J. F.; van Driel, H. M. Ambipolar diffusion of high-density electrons and holes in Ge, Si, and GaAs: Many-body effects. *Phys. Rev. B* **1982**, *26*, 2147−2158.
(58) Kane, D.; Swanson, R. The effect of excitons on apparent band gap narrowing and transport in semiconductors. *J. Appl. Phys.* **1993**, *73*, 1193−1197.
(59) Van Driel, H.; Preston, J.; Gallant, M. Confinement of laser-generated carriers in semiconductors by induced lattice temperature gradients. *Appl. Phys. Lett.* **1982**, *40*, 385−387.
(60) Guo, Y.; Wang, M. Phonon hydrodynamics and its applications in nanoscale heat transport. *Phys. Rep.* **2015**, *595*, 1−44.
(61) Guyer, R. A.; Krumhansl, J. A. Solution of the Linearized Phonon Boltzmann Equation. *Phys. Rev.* **1966**, *148*, 766−778.
(62) Beardo, A.; Pérez, L. A.; Sendra, L.; Alonso, M. I.; Melis, C.; Bafaluy, J.; Camacho, J.; Colombo, L.; Rurali, R.; Alvarez, F. X.; Reparaz, J. S. Observation of second sound in a rapidly varying temperature field in Ge. *Sci. Adv.* **2021**, *7*, No. eabg4677.
(63) Huberman, S.; Chen, K.; Song, B.; Chiloyan, V.; Ding, Z.; Maznev, A. A.; Chen, G.; Nelson, K. A. Observation of second sound in graphite at temperatures above 100 K. *Science* **2019**, *364*, 375−379.
(64) Beardo, A.; Calvo-Schwarzwälder, M.; Camacho, J.; Myers, T. G.; Torres, P.; Sendra, L.; et al. Hydrodynamic Heat Transport in Compact and Holey Silicon Thin Films. *Phys. Rev. Appl.* **2019**, *11*, No. 034003.
(65) Greffet, J.-J.; Bouchon, P.; Brucoli, G.; Marquier, F. Light Emission by Nonequilibrium Bodies: Local Kirchhoff Law. *Phys. Rev. X* **2018**, *8*, No. 021008.
(66) Song, B.; Fiorino, A.; Meyhofer, E.; Reddy, P. Near-field radiative thermal transport: From theory to experiment. *AIP Adv.* **2015**, *5*, No. 053503.
(67) Vázquez-Lozano, J. E.; Liberal, I. Incandescent temporal metamaterials. *Nat. Commun.* **2023**, *14*, 4606.
(68) Narayanaswamy, A.; Chen, G. Thermal near-field radiative transfer between two spheres. *Phys. Rev. B* **2008**, *77*, No. 075125.
(69) Ben-Abdallah, P.; Biehs, S.-A.; Joulain, K. Many-Body Radiative Heat Transfer Theory. *Phys. Rev. Lett.* **2011**, *107*, No. 114301.
(70) Joulain, K.; Ben-Abdallah, P.; Chapuis, P.-O.; Wilde, Y. D.; Babuty, A.; Henkel, C. Strong tip-sample coupling in thermal radiation scanning tunneling microscopy. *J. Quant. Spectrosc. Radiat. Transfer* **2014**, *136*, 1−15.
(71) Lundeberg, M. B.; Gao, Y.; Asgari, R.; Tan, C.; Van Duppen, B.; Autore, M.; Alonso-Gonzàlez, P.; Woessner, A.; Watanabe, K.; Taniguchi, T.; Hillenbrand, R.; Hone, J.; Polini, M.; Koppens, F. H. L. Tuning quantum nonlocal effects in graphene plasmonics. *ACS Nano* **2017**, *357*, 187.
(72) Ni, G. X.; McLeod, A. S.; Sun, Z.; Wang, L.; Xiong, L.; Post, K. W.; Sunku, S. S.; Jiang, B.-Y.; Hone, J.; Dean, C. R.; Fogler, M. M.; Basov, D. N. Fundamental limits to graphene plasmonics. *Nature* **2018**, *557*, 530.
(73) Zare, S.; Tajani, B. Z.; Edalatpour, S. Effect of nonlocal electrical conductivity on near-field radiative heat transfer between graphene sheets. *Phys. Rev. B* **2022**, *105*, No. 125416.
(74) Yang, F.; Song, B. Strong suppression of near-field thermal transport between twisted bilayer graphene near the magic angle. *Mater. Today Phys.* **2022**, *24*, No. 100692.
(75) Tang, G.; Zhang, L.; Zhang, Y.; Chen, J.; Chan, C. T. Near-Field Energy Transfer between Graphene and Magneto-Optic Media. *Phys. Rev. Lett.* **2021**, *127*, No. 247401.
(76) Wu, H.; Huang, Y.; Cui, L.; Zhu, K. Active Magneto-Optical Control of Near-Field Radiative Heat Transfer between Graphene Sheets. *Phys. Rev. Appl.* **2019**, *11*, No. 054020.
(77) Yang, B.; Song, B.; de Abajo, F. J. G.; Dai, Q. Ultrafast Thermal Switching Enabled by Transient Polaritons. *ACS Nano* **2025**, *19*, 1490−1498.
(78) Park, K.-D.; May, M. A.; Leng, H.; Wang, J.; Kropp, J. A.; Gougousi, T.; Pelton, M.; Raschke, M. B. Tip-enhanced strong coupling spectroscopy, imaging, and control of a single quantum emitter. *Sci. Adv.* **2019**, *5*, No. eaav5931.
(79) Chikkaraddy, R.; de Nijs, B.; Benz, F.; Barrow, S. J.; Scherman, O. A.; Rosta, E.; Demetriadou, A.; Fox, P.; Hess, O.; Baumberg, J. J. Single-molecule strong coupling at room temperature in plasmonic nanocavities. *Nature* **2016**, *535*, 127−130.
(80) Bistritzer, R.; MacDonald, A. H. Electronic Cooling in Graphene. *Phys. Rev. Lett.* **2009**, *102*, No. 206410.
(81) Graham, M. W.; Shi, S.-F.; Ralph, D. C.; Park, J.; McEuen, P. L. Photocurrent measurements of supercollision cooling in graphene. *Nat. Phys.* **2013**, *9*, 103−109.
(82) Betz, A. C.; Jhang, S. H.; Pallecchi, E.; Ferreira, R.; Fève, G.; Berroir, J.-M.; Plaçais, B. Supercollision cooling in undoped graphene. *Nat. Phys.* **2013**, *9*, 109−112.
(83) Mihnev, M. T.; Kadi, F.; Divin, C. J.; Winzer, T.; Lee, S.; Liu, C.-H.; Zhong, Z.; Berger, C.; de Heer, W. A.; Malic, E.; Knorr, A.;

Norris, T. B. Microscopic origins of the terahertz carrier relaxation and cooling dynamics in graphene. *Nat. Commun.* **2016**, *7*, No. 11617.
(84) Chen, Y.; Li, Y.; Zhao, Y.; Zhou, H.; Zhu, H. Highly efficient hot electron harvesting from graphene before electron-hole thermalization. *Sci. Adv.* **2019**, *5*, No. eaax9958.
(85) Pogna, E. A. A.; et al. Hot-Carrier Cooling in High-Quality Graphene Is Intrinsically Limited by Optical Phonons. *ACS Nano* **2021**, *15*, No. 11285.
(86) Hanson, G. W. Dyadic Green's functions and guided surface waves for a surface conductivity model of graphene. *J. Appl. Phys.* **2008**, *103*, No. 064302.
(87) Hardy, R. J. Phonon Boltzmann Equation and Second Sound in Solids. *Phys. Rev. B* **1970**, *2*, 1193−1207.
(88) Ackerman, C. C.; Bertman, B.; Fairbank, H. A.; Guyer, R. A. Second Sound in Solid Helium. *Phys. Rev. Lett.* **1966**, *16*, 789−791.
(89) Narayanamurti, V.; Dynes, R. C. Observation of Second Sound in Bismuth. *Phys. Rev. Lett.* **1972**, *28*, 1461−1465.
(90) McNelly, T. F.; Rogers, S. J.; Channin, D. J.; Rollefson, R. J.; Goubau, W. M.; Schmidt, G. E.; et al. Heat Pulses in NaF: Onset of Second Sound. *Phys. Rev. Lett.* **1970**, *24*, 100−102.
(91) McBennett, B.; Beardo, A.; Nelson, E. E.; Abad, B.; Frazer, T. D.; Adak, A.; et al. Universal Behavior of Highly Confined Heat Flow in Semiconductor Nanosystems: From Nanomeshes to Metalattices. *Nano Lett.* **2023**, *23*, 2129−2136.
(92) Shang, M.-Y.; Zhang, C.; Guo, Z.; Lü, J.-T. Heat vortex in hydrodynamic phonon transport of two-dimensional materials. *Sci. Rep.* **2020**, *10*, 8272.
(93) Simoncelli, M.; Marzari, N.; Cepellotti, A. Generalization of Fourier's Law into Viscous Heat Equations. *Phys. Rev. X* **2020**, *10*, No. 011019.
(94) Cepellotti, A.; Marzari, N. Boltzmann Transport in Nanostructures as a Friction Effect. *Nano Lett.* **2017**, *17*, 4675−4682.
(95) Cui, L.; Hur, S.; Akbar, Z. A.; Klöckner, J. C.; Jeong, W.; Pauly, F. Thermal conductance of single-molecule junctions. *Nature* **2019**, *572*, 628−633.
(96) Vermeersch, B.; Carrete, J.; Mingo, N.; Shakouri, A. Superdiffusive heat conduction in semiconductor alloys. I. Theoretical foundations. *Phys. Rev. B* **2015**, *91*, No. 085202.
(97) Zenji, A.; Pernot, G.; Lacroix, D.; Rampnoux, J. M.; Bourgeois, O.; Grauby, S.; Dilhaire, S. Seeking non-Fourier heat transfer with ultrabroad band thermoreflectance spectroscopy. *Commun. Mater.* **2024**, *5*, No. 123.
(98) Lucas, A.; Fong, K. C. Hydrodynamics of electrons in graphene. *J. Phys.: Condens. Matter* **2018**, *30*, No. 053001.
(99) Varnavides, G.; Jermyn, A. S.; Anikeeva, P.; Felser, C.; Narang, P. Electron hydrodynamics in anisotropic materials. *Nat. Commun.* **2020**, *11*, 4710.

https://doi.org/10.1021/acsnano.4c11893
ACS Nano 2025, 19, 6033−6043